Article

A High Signal Noise Ratio UWB Radar for Buried Pipe Location Using Golay Complementary Sequences

Jingxia Li [1,2,*], Yang Liu [1,2], Hang Xu [1,2], Bingjie Wang [1,2], Li Liu [1,2] and Xinpeng Chen [1,2]

[1] Key Laboratory of Advanced Transducers & Intelligent Control System, Ministry of Education and Shanxi Province, Taiyuan University of Technology, Taiyuan 030024, China; m15534214105_1@163.com (L.Y.); xuhang@tyut.edu.cn (X.H.); wangbingjie@tyut.edu.cn (B.W.); liuli01@tyut.edu.cn (L.L.); chenxinpeng0865@link.tyut.edu.cn (X.C.);

[2] College of Physics & Optoelectronics, Taiyuan University of Technology, Taiyuan 030024, China;

* Correspondence: lijingxia@tyut.edu.cn; Tel.: +86-351-601-8249 (J.L.)

Abstract: An experimental ultra wideband ground penetrating radar based on Golay complementary sequences is proposed to locate underground pipes. Golay complementary sequences with the code length of 1024 and frequency of 1 GHz are used as the probe signals. Two-dimensional image of the buried pipes is achieved by correlation method and back projection algorithm. The experimental results show that both the plastic pipe and metallic pipe can be located with a range resolution of 10 cm. Furthermore, as the Golay complementary sequences are a pair of complementary sequences, the sum of their correlation function yields twice the value of the peak at the target position and zero elsewhere. Thus, compared with the stepped frequency signal radar or chaotic signal radar, the Golay-based radar can significantly improve the signal noise ratio and has capability of deep detection.

Keywords: Golay complementary sequences; sidelobes; pipe detection; chaotic signal

1. Introduction

Detection and location of underground pipes before excavation works is extremely important to ensure faultless working processes and minimize the impacts to the existing pipes in the intervention area. Once the buried pipes are damaged, the undesirable fluid losses due to leaks can cause enormous environmental and economic repercussions. Ultra wideband ground penetrating radar (UWB GPR) [1-3] as one of the non-destructive techniques [4-8] to locate the underground pipes attracts increasing attention because it is capable of accurately locating both metallic and non-metallic pipes without prior knowledge. However, conventional UWB GPR utilizes short pulse as the transmit signals, which has to compromise between the resolution and the detection distance.

In order to expand the detectable range without degrading the resolution, large time-bandwidth signals are used as the transmit signals in recent years, such signals include frequency modulated continuous wave (FMCW) signals [9-11], stepped frequency signals [12-14], code signals [15-17], and chaotic signals [18-20]. UWB GPR based on FMCW signals or stepped frequency signals suffers from having strong sidelobes [21], thereby resulting in low signal noise ratio (SNR). To suppress these undesired sidelobes, different mismatched filters have been reported in the literature [22-24]. Unfortunately, these sidelobes suppression techniques come at the cost of SNR loss and resolution reduction [25]. Pseudo random binary sequences (PRBS or m-sequences) have low sidelobes and exhibit good correlation properties. Additionally, their sidelobes can be further reduced by extending the length of the PRBS [26]. Thus, the UWB GPR based PRBS can enhance the SNR [27]. Extensive studies show chaotic signals possess many properties that make them an attracting candidate for radar system design. The random nature of chaotic signals shows good correlation properties, which can improve the SNR of radar [31]. Although, both PRBS and

chaotic signals are considered good options in terms of their low sidelobes, these two signals are not ideal choice if sidelobe level is taken into account. Golay complementary sequences are a pair of equal length sequences that have the following property: when their correlation functions are algebraically added, their sidelobes are cancelled while the correlation peak is double of that individual one [32]. Therefore, the Golay complementary sequences are very suitable for UWB GPR.

In this paper, high speed Golay complementary sequences are achieved and applied to underground pipe detection. Experimental results demonstrate that plastic pipe and metallic pipe can be located with a range resolution of 10 cm. Furthermore, compared with the stepped frequency signal radar or chaotic signal radar, the Golay complementary sequences radar system can significantly improve the SNR, thereby improving the detection depth of the system. This paper is organized as follows: Section 2 provides the radar system and its measure principle. Section 3 describes the generation and characteristics of the Golay complementary sequences. Section 4 shows the experimental results on underground pipe location. Section 5 shows the comparison results among proposed radar, chaotic radar and stepped frequency signal radar. Finally, conclusions are given in Section 6.

2. Radar System and Measure Principle

The experimental setup of the underground pipe locating utilizing the Golay complementary sequences is shown in Figure 1. The signal source generates a pair of high speed Golay complementary sequences: sequence A and sequence B. Then the sequence A or sequence B is split into two paths. One serves as the reference signal recorded by a real-time oscilloscope (RTO1024, ROHDE&SCHWARZ, Munich, Germany). The other is amplified by a 25 dB amplifier 1 (KG-RF-10, CONQUER, Beijing, China). After being up-converted by a mixer 1 (M2-0026, Marki, Morgan Hill, CA, USA) and amplified by a 10 dB amplifier 2, it is then transmitted by a wideband horn antenna (TX, LB-10180, A-INFO, Chengdu, China) with an operating frequency range of 1 GHz to 18 GHz and a reported gain of 11 dBi. The echo signal is received by a wideband horn antenna (RX). After being amplifier by a 20 dB gain amplifier 3 (KG-RF-10, CONQUER), down-converted by a mixer 2, and amplified by a low noise amplifier 4 (1190A, Agilent, Santa Clara, CA, USA), the echo signal is record by the oscilloscope and then the outputs of the oscilloscope are transferred to a computer for data processing and display. In the experiment, the average power of the probe signal is -12 dBm. The signal generator (AV1487A, CETC, Qingdao, China) is used to provide 3.4 GHz local oscillator frequency for mixer 1 and mixer 2.

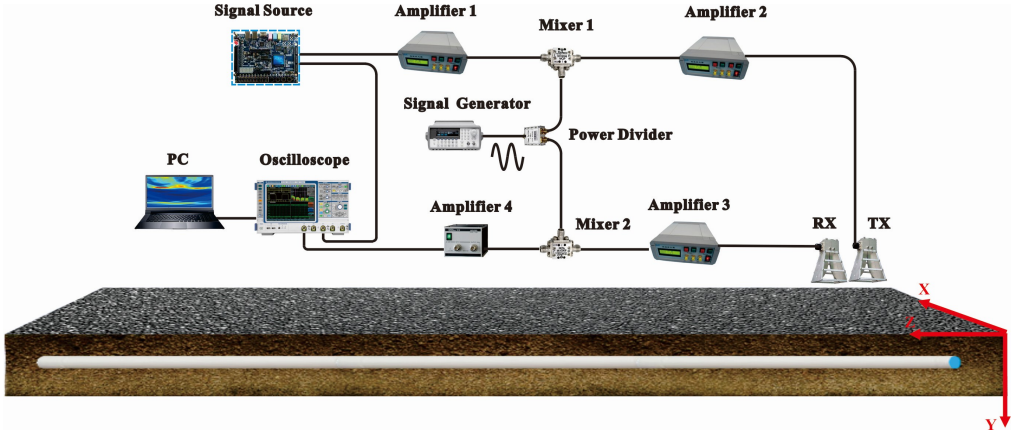

Figure 1. Block diagram of the Golay complementary sequences radar system.

The proposed radar system utilizes a pair of high speed Golay complementary sequences as the probe signals. The Golay-based radar can obtain the depth of buried pipe by correlated the corresponding reference signal and the echo signal. The respective correlation functions are given by:

$$V_{Acorr}(t) = V_{Aref}(t) \otimes V_{Aech}(t) = k\delta(t-\tau), \quad (1)$$

$$V_{Bcorr}(t) = V_{Bref}(t) \otimes V_{Bech}(t) = k\delta(t-\tau), \quad (2)$$

where $\otimes$ is correlation operator, τ is the time delay between the echo signal and the reference, and k is the system related constant. $V_{Acorr}(t)$, $V_{Aref}(t)$, and $V_{Aech}(t)$ denote the correlation signal, reference signal, and echo signal of sequence A, respectively. $V_{Bcorr}(t)$, $V_{Bef}(t)$, and $V_{Bech}(t)$ denote the correlation signal, reference signal, and echo signal of sequence B, respectively. We can obtain the buried depth of pipe from the position of the correlation peak.

Although the depth of the pipe can be obtained from either correlation of sequence A or correlation of sequence B. However, by adding the correlation of sequence A to the correlation of complementary sequence B, we can obtain that the sum of the two correlation functions has a peak value of twice code length and a sidelobe level of zero, which is beneficial for pipe location. The sum of the two correlations $V_{A+B}(t)$ is given by:

$$V_{A+B}(t) = 2k\delta(t-\tau), \quad (3)$$

Then back projection (BP) algorithm is used to achieve the two-dimensional (2D) imaging of the pipe. The TX and RX with a constant spacing move along a line. The whole imaging region is divided into P pixels. For any pixel point p, the signal $I_P(t)$ equals the sum of all envelopes of $V_{A+B}(t)$ at the corresponding time delay. $I_P(t)$ can be written as:

$$I_p(t) = \sum_{n=1}^{M} \left| V_{A+B}(t) \right| \delta(t - \frac{2R_{np}}{v}), \quad (4)$$

where R_{np} is the distance from pixel p to the n-th TX/RX, v is the velocity of underground wave, M is the unite of array elements. If the pipe is located at pixel p, the energy at this position will be enhanced. Otherwise it will be small and can be regarded as the background. The entire imaging area I can be written as:

$$I = \sum_{p=1}^{P} I_p(t), \quad (5)$$

3. Generation and Characteristics of the Probe Signal

The Golay complementary sequences are generated from a field programmable gate array (FPGA, intel Cyclone V 5CG) and the corresponding hardware structure diagram is shown in Figure 2. The source generator generates a pair of low speed Golay complementary sequences: sequence A and sequence B. Their code lengths are controlled by the variable controller. Through the multiplexer (MUX), sequence A or sequence B is selected and then sent into serializer, which is used to convert data into large bitwidth parallel data. The large bitwidth data is stored in the static random access memory (SRAM) using a SRAM controller. When the transceiver receives a reset signal from the reset controller, it controls the SRAM controller and reads the data. After deserializing in the transceiver, the data is output through the low-voltage differential signaling (LVDS) interface to obtain a high-speed Golay complementary code. In the hardware implementation diagram, the reconfiguration controller is used to adjust the signal transmission rate. Utilizing this FPGA board, we can generate a pair of Golay complementary sequences with a maximum code length of 2^{19} and tunable frequency between 615 MHz and 3.125 GHz. In actual use, the signal frequency and code length can be flexibly selected according to the requirements of the detection environment. In our experiment, the code length and the frequency of the Golay complementary sequences are 1024 and 1 GHz, respectively.

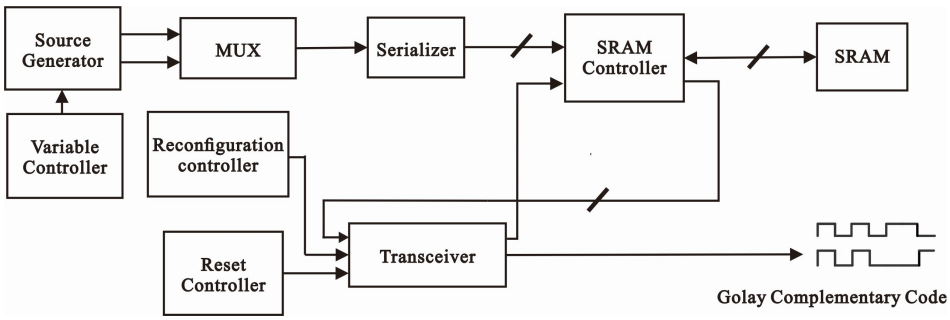

Figure 2. Hardware implementation diagram of the Golay complementary sequences.

Figure 3 and Figure 4 show the properties of Golay complementary sequences. The time series of a pair of Golay complementary sequences are shown in Figure 3a and Figure 3b. The amplitude of sequences A and complementary sequences B are 0.1 V, and a symbol period of each sequences is 1 ns. Figure 3c and Figure 3d show the corresponding power spectrums of sequences A and B, respectively. The autocorrelation of each sequence is shown in Figure 4. The individual autocorrelation of A or B exhibits sidelobes. However, when the two autocorrelations are added together, the peak value is twice its single autocorrelation, whereas the sidelobes cancel exactly.

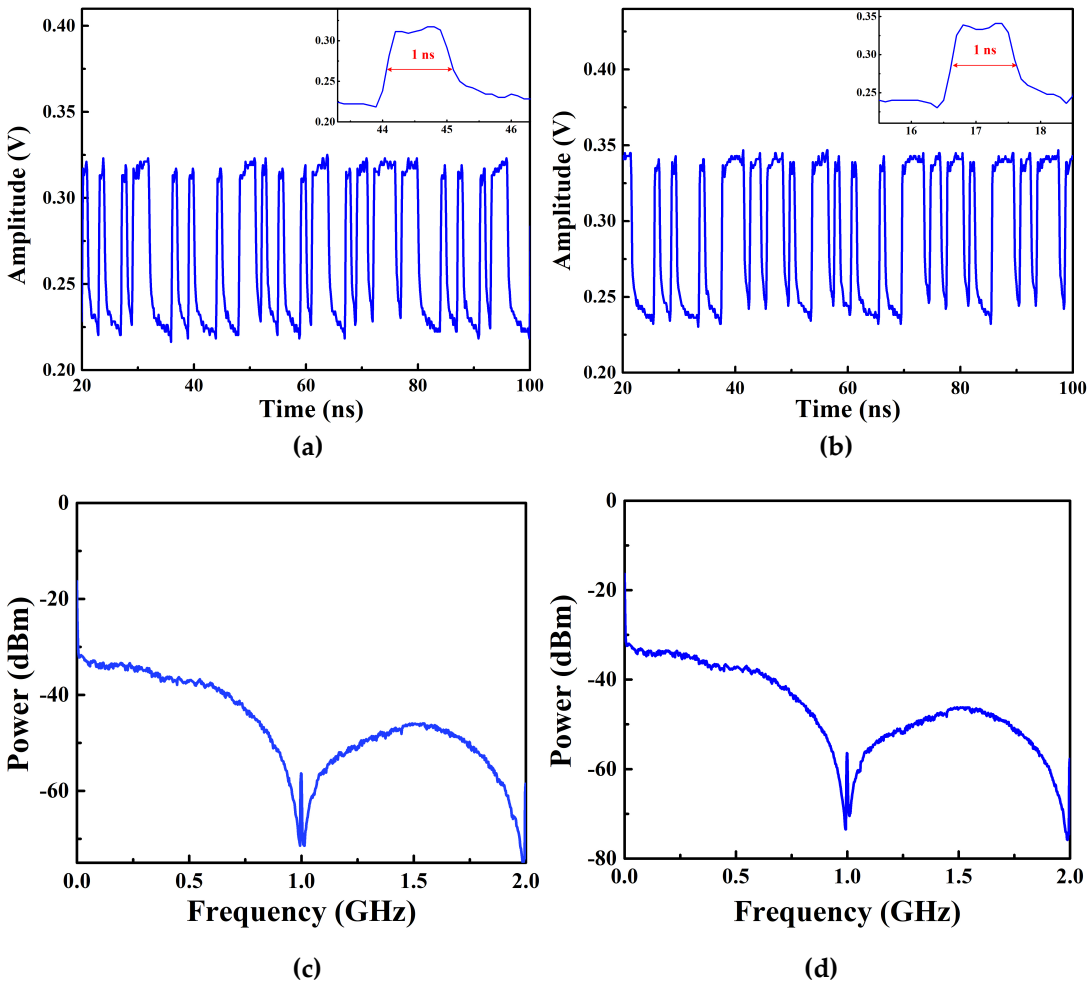

Figure 3. Time series of (a) sequences A and (b) complementary sequences B. Power spectrum of (c) sequences A and (d) complementary sequences B.

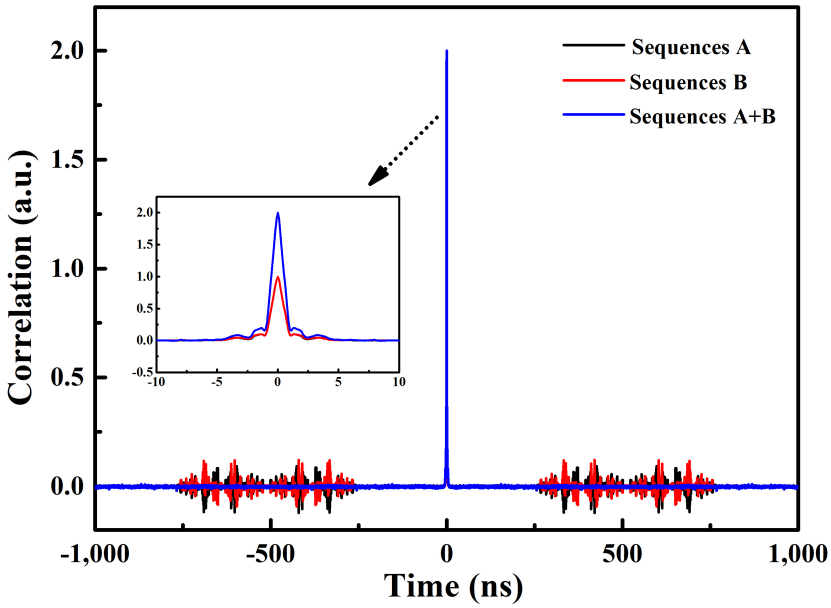

Figure 4. Autocorrelation traces of sequences A, complementary sequences B, and sequences A+ sequences B.

4. Experimental Results

We experimentally locate underground pipe utilizing Golay complementary sequences. A tank filled with dry sand is used to simulate experimental scenario. It is 2.00 m×1.50 m×1.50 m size and made of acrylic with steel structure. Absorbing materials are attached to the surface of the steel to eliminate the strong interference of the steel. In the experiment, the TX and RX are placed on the surface of the sand with the distance between TX and RX of 2 cm. They are moved along the x-axis with a step size of 5 cm, as shown in Figure 1. In addition, average filtering is applied to inhibit the direct wave reflected from the surface and crosstalk between TX and RX. The wave velocity in our experiment is about 2×10^8 m/s, which is deduced from the delay time and the known-depth of the pipe. The range resolution of the system is about 10 cm. It is estimated by $v/2B$, where v is the wave velocity of electromagnetic wave in the transmission media, B is the bandwidth of the signal. The parameters of the pipes used in the experimental are shown in Table 1. All of these pipes are filled by air.

Table 1. Summary of materials, diameters, length and depths employed in the experiment.

Pipes	Material	Diameter (m)	Length (m)	Thickness (mm)
P1	Plastic	0. 20	0.52	3
P2	Plastic	0.15	0.60	4
M1	Metallic	0.10	0.60	2
M2	Metallic	0.05	0.35	1

The experimental results are shown in Figure 5. The circles in the figure represent the actual profile of pipes. The co-ordinates corresponds the top position of the buried pipe. We first locate two plastic pipes (P1 and P2) buried 85 cm and 60 cm below the sand surface. The location result is shown in Figure 5a, which demonstrates plastic pipes buried at different depth can be located. In Figure 5a, the reflection appearing at a depth of approximately 135 cm is from the steel of tank bottom. Similarly, when two metallic pipes (M1 and M2) buried at different depth, from the corresponding 2D image, we can also clearly identified their positions. Furthermore, to give a better description of the real condition, we locate two different material pipes (P1 and M2) simultaneously. Figure 5c shows that both the positions of the plastic pipe and metallic pipe can be visible and each position accords with the real value. The above results demonstrate that the Golay complementary

sequences can successfully be applied to locate underground pipes. In addition, from Figure 5b and Figure 5c we can observe that due to the existence of the metallic pipe, the reflection of the other pipe around metallic one will be weakened.

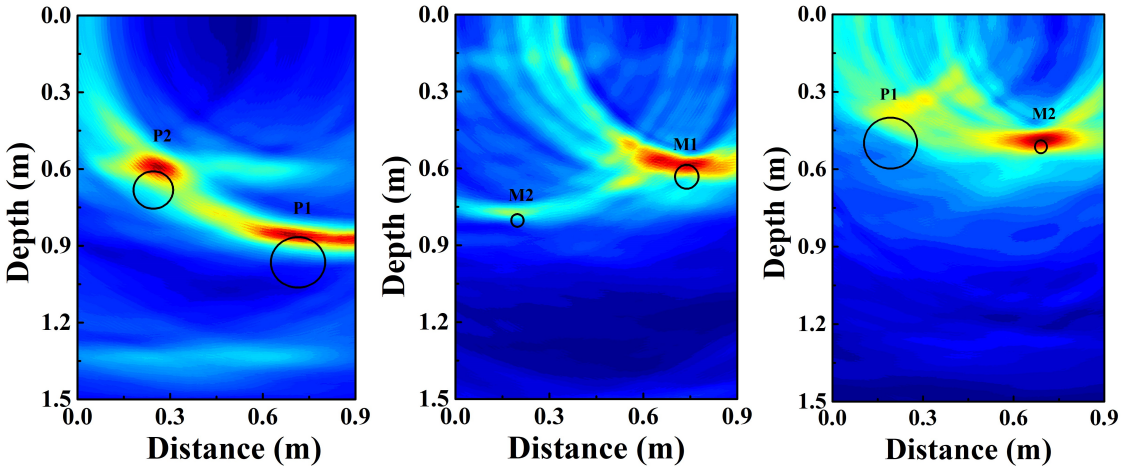

Figure 5. The radar profile of buried pipes. (a) P2 and P1 at position of (23, 60) cm and (72, 85) cm. (b) M2 and M1 at position of (20, 78) cm and (72, 57) cm. (c) Two different type pipes at position of (18, 40) m and (68, 49) cm.

5. Detection Performance

To analyze the performance of the proposed Golay complementary sequences radar system, we give the comparison among the proposed radar, chaotic radar, and stepped frequency signal radar. Here, the vector network analyzer is regarded as the stepped frequency signal radar whose modulated frequency range is from 1.80 GHz to 5.00 GHz. The chaotic radar is based on chaotic pulse position modulation (CPPM) signal. CPPM is used to generate a sequence of pulse distanced by time intervals generated by a chaotic map [33]. Compared with chaotic pulse amplitude modulation signal, it has low crest factor and thus has a great robustness to external noise [34]. We have detailed descried CPPM signal radar in our previous work [35]. In this experiment, the CPPM signal with 1.00 GHz bandwidth is up-converted to 2.40 GHz - 4.40 GHz. Then we use the up-converted signal as the probe signal. Besides, other parameters in these three radar systems are the same, such as the transmitting power, the distance between the two antennas, the step of two antennas and pipe parameters.

Figure 6 shows comparison result of normalization curves. Plastic pipe is buried at 40 cm in three radar systems. In the normalization curves, the peak position presents the buried depth of the pipe. The higher of this peak, the easier it is to identify the target. Thus, observing Figure 6, we obtain that the peak of the curve based on Golay complementary sequences is remarkable higher than that based on CPPM signal or stepped frequency signal, when the pipe is buried at the same depth. Besides, by using chaotic radar and Golay-based radar, the reflection of tank bottom at 120 cm can also be clearly observed. While it cannot be obtained by using stepped frequency signal radar.

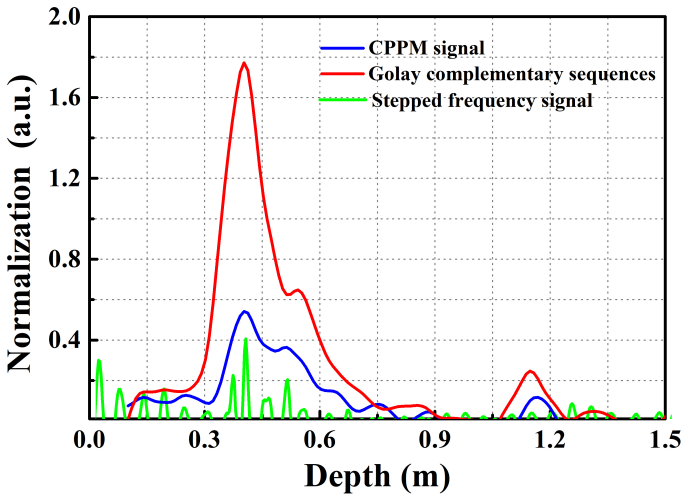

Figure 6. Normalization curves of three different types radar systems.

We analyze the relationship between signal noise ratio (SNR) of the normalization curve and the buried depth, as shown in Figure 7. The SNR is defined as follows [36]:

$$SNR = 20\log\frac{A_s}{A_n}, \tag{6}$$

where A_S refers to the amplitude of the target reflection peak and A_N refers to the amplitude of the maximum noise peak. From Figure 7a or Figure 7b we can see that the SNR obtained from the Golay complementary sequences radar is also higher than that of CPPM signal radar or stepped frequency signal radar at the same buried depth, no matter whether the target is plastic pipe or metallic pipe. The results mean the proposed radar system is capable of detecting deeper buried pipe. Additionally, the SNRs of stepped frequency signal radar, CPPM signal radar, and Golay-based radar at 40 cm (correspond to the results in Figure 6) are 2.65 dB, 6.61 dB, and 13.44 dB, respectively.

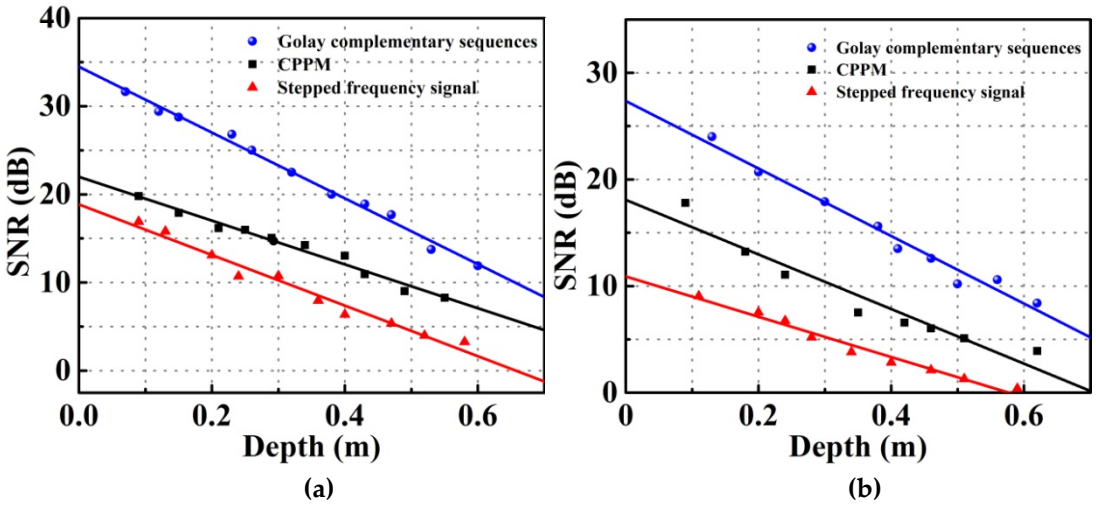

Figure 7. The SNRs of (a) metallic pipe and (b) plastic pipe as the function of buried depth.

Furthermore, to intuitive analysis of the performance of these three radar systems in underground pipe location, 2D images are given. Figure 8a, Figure 8b, and Figure 8c show the 2D images of stepped frequency signal radar, chaotic radar, and Golay complementary sequences radar, respectively, when the same plastic pipe is buried at about 60 cm. Comparing the figures, we can see that although the position of plastic pipe can be observed in these three figures, Figure 8c shows the

greatest contract between the plastic pipe and the surroundings. It means the value at this position is the largest in these three figures, which is beneficial to locate deeper buried pipe. And this result is consistent with previous conclusions obtained from Figure 6 and Figure 7.

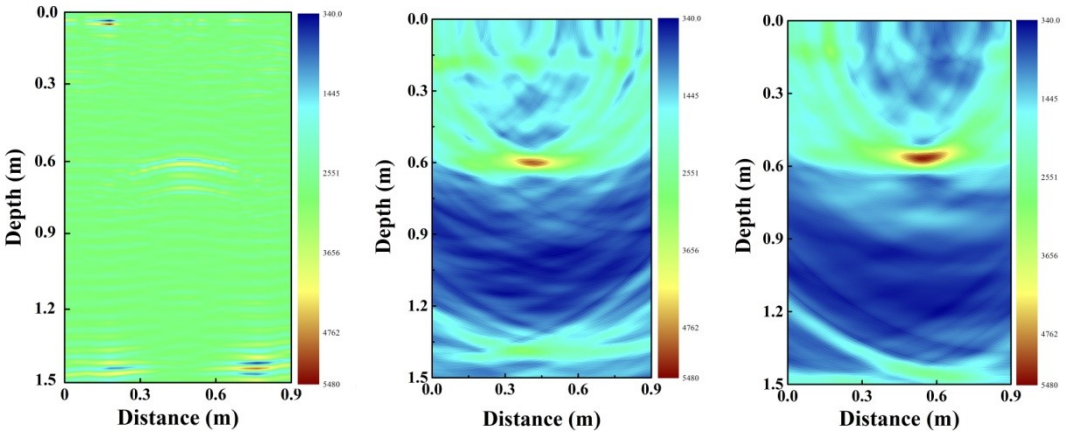

Figure 8. Plastic pipe location based on (a) stepped frequency signal radar, (b) chaotic signals radar, and (c) Golay complementary sequences radar.

6. Conclusions

High speed Golay complementary sequences are applied to GPR for underground pipe location. The buried pipe is located by correlation method and BP algorithm. Experimental results show that metallic pipe and plastic pipe detected and the range resolution is 10 cm. Golay complementary sequences are a pair of complementary sequences. By adding the correlation of the two complementary sequences, we can obtain that the sum of the two correlation functions has a peak value of twice code length and a sidelobe level of zero. Therefore, compared with Golay complementary sequences radar with stepped frequency signal radar or chaotic signal radar, the Golay-based radar has higher SNR, which is beneficial for deep buried pipe location. Besides, the signal rate and code length of the Golay complementary sequences can be flexibly selected according to the requirements of the detection environment.

Author Contributions: Conceptualization, methodology, writing-original draft preparation, J.L.; Investigation, Y.L.; writing-review & editing, formal analysis, H.X.; project administration, L.L.; resources, B.W.; data curation, X.C.

Funding: This research was funded by the National Natural Science Foundation of China, grant numbers 41604127, 41704147, 61601319, and 61705007; The Natural Science Foundation of Shanxi Province, grant numbers 201801D221185, 201701D221114, 201801D121140, and 201701D121009; The Key Research and Development (R&D) Projects of Shanxi Province, grant numbers 201703D321036 and 201803D31037; The Shanxi Key research and development Foundation of China, grant numbers 201803D121057; The China Scholarship Council (CSC) , grant numbers 201806935029.

Conflicts of Interest: The authors declare no conflict of interest.

References

1. Brunzell, H. Detection of shallowly buried objects using impulse radar. *IEEE Transactions on Geoscience and Remote Sensing* **1999**, 37, 875–886. https://ieeexplore.ieee.org/abstract/document/752207
2. Agrawal, S.; George, N.V.; Prashant, A. GPR data analysis of weak signals using modified s-transform. *Geotechnical and Geological Engineering* **2015**, *33*, 1167-1182. https://link.springer.com/article/10.1007/s10706-015-9893-5

3. Huuskonen-Snicker, E.; Mikhnev, V.A.; Olkkonen, M.K. Discrimination of buried objects in impulse GPR using phase retrieval technique. *IEEE Transactions on Geoscience and Remote Sensing* **2015**, *53*, 1001-1007. https://ieeexplore.ieee.org/abstract/document/6851164
4. Rifai, D.; Abdalla, A.; Razali, R.; Ali, K.; Faraj, M. An eddy current testing platform system for pipe defect inspection based on an optimized eddy current technique probe design. *Sensors* **2017**, *17*, 579. https://www.mdpi.com/1424-8220/17/3/579
5. Saha, S.; Mukhopadhyay, S.; Mahapatra, U.; Bhattacharya, S.; Srivastava, G.P. Empirical structure for characterizing metal loss defects from radial magnetic flux leakage signal. *Ndt & E International* **2010**, *43*, 507–512. https://www.sciencedirect.com/science/article/pii/S0963869510000599
6. Xue, Q.; Leung, H.; Huang, L.; Zhang, R.; Liu, B.; Wang, J.; Li, L. Modeling of torsional oscillation of drillstring dynamics. *Nonlinear Dynamics* **2019**, 96, 267-283. https://doi.org/10.1007/s11071-019-04789-x
7. Choi, M.; Kang, K.; Park, J.; Kim, W.; Kim, K. Quantitative determination of a subsurface defect of reference specimen by lock-in infrared thermography. *Ndt & E International* **2008**, *41*, 119–124. https://www.sciencedirect.com/science/article/pii/S096386950700103X
8. Gao, Y.; Brennan, M.; Joseph, P.F.; Muggleton, J.M.; Hunaidi, O. On the selection of acoustic/vibration sensors for leak detection in plastic water pipes. *Journal of Sound and Vibration* **2005**, *283*, 927-941. https://www.sciencedirect.com/science/article/pii/S0022460X04005358
9. Detlefsen, J.; Dallinger, A.; Schelkshorn, S.; Bertl S. UWB millimeter-wave FMCW radar using hubert transform methods. 2006 IEEE Ninth International Symposium on Spread Spectrum Techniques and Applications, Manaus Amazon, Brazil, 28-31 August 2006, pp. 46-48. https://ieeexplore.ieee.org/abstract/document/4100520/authors
10. Gierlich, R.; Huettner, J.; Ziroff, A.; Weigel, R.; Huemer, M. A reconfigurable MIMO system for high-precision FMCW local positioning. *IEEE Transactions on Microwave Theory and Techniques* **2011**, 59, 3228-3238. https://ieeexplore.ieee.org/abstract/document/6046106/authors#authors
11. Lee, H.; Kim, B.H.; Park, J.K.; Yook, J.G. A Novel Vital-Sign Sensing Algorithm for Multiple Subjects Based on 24-GHz FMCW Doppler Radar. *Remote Sensing* **2019**, 11, 1237. https://www.mdpi.com/2072-4292/11/10/1237
12. Wu, Y.; Shen, F.; Yuan, Y.; Xu, D. An Improved Modified Universal Ultra-Wideband Antenna Designed for Step Frequency Continuous Wave Ground Penetrating Radar System. *Sensors* **2019**, 19, 1045. https://www.mdpi.com/1424-8220/19/5/1045
13. Phelan, B.R.; Ranney, K.I.; Gallagher, K.A.; Clark, J.T.; Sherbondy, K.D.; Narayanan, R.M. Design of ultrawideband stepped-frequency radar for imaging of obscured targets. *IEEE Sensors Journal* **2017**, 17, 4435-4446. https://ieeexplore.ieee.org/abstract/document/7932846/authors#authors
14. Wang, H.; Dang, V.; Ren, L.; Liu, Q.; Ren, L.; Mao, E.; Kilik, O.; Fathy, A.E. An elegant solution: an alternative ultra-wideband transceiver based on stepped-frequency continuous-wave operation and compressive sensing. *IEEE Microwave Magazine* **2016**, 17, 53-63. https://ieeexplore.ieee.org/abstract/document/7484804/authors#authors
15. Liu, X.; Yan, K.; Chen, Z.; Li, C.; Zhang, J.; Ye, S.; Fang, G. A m-sequence UWB radar system design and contrast test with an impulse radar. 2018 IEEE 17th International Conference on Ground Penetrating Radar (GPR), Rapperswil, Switzerland, 18-21 June 2018, pp. 1-4. https://ieeexplore.ieee.org/abstract/document/8441647/authors#authors
16. Sachs, J.; Herrmann, R. M-sequence-based ultra-wideband sensor network for vitality monitoring of elders at home. *IET Radar, Sonar & Navigation* **2015**, 9, 125-137. https://digital-library.theiet.org/content/journals/10.1049/iet-rsn.2014.0214
17. Xia, Z.; Fang, G.; Ye, S.; Zhang, Q.; Chen, C.; Yin, H. A novel handheld pseudo random coded UWB radar for human sensing applications. *IEICE Electronics Express* **2014**, 11, 20140981. https://www.jstage.jst.go.jp/article/elex/advpub/0/advpub_11.20140981/_article/-char/ja/
18. Lin F.Y.; Liu J.M. Chaotic radar using nonlinear laser dynamics. *IEEE Journal of Quantum Electronics* **2004**, 40, 815-820. https://ieeexplore.ieee.org/abstract/document/1303798
19. Shi, Z.G.; Qiao, S.; Chen, K.S.; Cui, W.Z.; Ma, W.; Jiang, T.; Ran, L.X. Ambiguity functions of direct chaotic radar employing microwave chaotic Colpitts oscillator. *Progress In Electromagnetics Research* **2007**, 77, 1-14. http://www.jpier.org/PIER/pier.php?paper=07072001

20. Esmaeili-Najafabadi, H.; Ataei, M.; Sabahi, M.F. Designing sequence with minimum PSL using Chebyshev distance and its application for chaotic MIMO radar waveform design. *IEEE Transactions on Signal Processing* **2016**, 65, 690-704. https://ieeexplore.ieee.org/abstract/document/7707413/authors
21. Levanon, N.; Scharf, A. Range sidelobes blanking by comparing outputs of contrasting mismatched filters. *IET radar, sonar & navigation* **2009**, 3, 265-277. https://ieeexplore.ieee.org/abstract/document/5071509/authors#authors
22. Cooper, K.B.; Durden, S.L.; Cochrane, C.J.; Monje, R.R.; Dengler, R.J.; Baldi, C. Using FMCW doppler radar to detect targets up to the maximum unambiguous range. *IEEE Geoscience and Remote Sensing Letters* **2017**, 14, 339-343. https://ieeexplore.ieee.org/abstract/document/7812583/authors#authors
23. Yan, J.B.; Alvestegui, D.G.G.; McDaniel, J.W.; Li, Y.; Gogineni, S.; Rodriguez-Morales, F.; Brozena, J.; Leuschen, C.J. Ultrawideband FMCW radar for airborne measurements of snow over sea ice and land. *IEEE Transactions on Geoscience and Remote Sensing* **2016**, 55, 834-843. https://ieeexplore.ieee.org/abstract/document/7723845/authors#authors
24. Hitzler, M.; Saulig, S.; Boehm, L.; Mayer, W.; Winkler, W.; Uddin, N.; Waldschmidt, C. Ultracompact 160-GHz FMCW radar MMIC with fully integrated offset synthesizer. *IEEE Transactions on Microwave Theory and Techniques* **2017**, 65, 1682-1691. https://ieeexplore.ieee.org/abstract/document/7845617/authors#authors
25. Collins, T.; Atkins, P. Nonlinear frequency modulation chirps for active sonar. *IEE Proceedings-Radar, Sonar and Navigation* **1999**, 146, 312-316. https://digital-library.theiet.org/content/journals/10.1049/ip-rsn_19990754
26. Hewitt, A.; Vilar, E. Selective fading on LOS microwave links: Classical and spread-spectrum measurement techniques. *IEEE transactions on communications* **1988**, 36, 789-796. https://ieeexplore.ieee.org/abstract/document/2807/authors#authors
27. Arai, I.; Tomizawa, Y.; Hirose, M. Pulse compression subsurface radar. *IEICE Transactions on Communications* **2000**, *83*, 1930-1937. https://search.ieice.org/bin/summary.php?id=e83-b_9_1930
28. Venkatasubramanian, V.; Leung, H.; Liu, X. Chaos UWB radar for through-the-wall imaging. *IEEE Transactions on Image Processing* **2009**, *18*, 1255-1265. https://ieeexplore.ieee.org/abstract/document/4895342
29. Zhang, M.; Ji, Y.; Zhang, Y.; Wu, Y.; Xu, H.; Xu, W. Remote radar based on chaos generation and radio over fiber. *IEEE Photonics journal* **2014**, *6*, 1-12. https://ieeexplore.ieee.org/abstract/document/6894267
30. Liu, L.; Guo, C.; Li, J.; Xu, H.; Zhang, J.; Wang, B. Simultaneous life detection and localization using a wideband chaotic signal with an embedded tone. *Sensors* **2016**, *16*, 1866.
31. Wang, B.; Zhao, T.; Wang, H. Improvement of signal-to-noise ratio in chaotic laser radar based on algorithm implementation. *Chinese Optics Letters* **2012**, 10, 052801. https://www.osapublishing.org/col/abstract.cfm?uri=col-10-5-052801
32. Budišin, S.Z. Efficient pulse compressor for Golay complementary sequences. *Electronics Letters* **1991**, 27, 219-220. https://digital-library.theiet.org/content/journals/10.1049/el_19910142
33. Xu, H.; Wang, B.; Zhang, J.; Liu, L.; Wang, Y.; Wang, A. Chaos through-wall imaging radar. *Sensing and Imaging* **2017**, 18, 6. https://link.springer.com/article/10.1007/s11220-017-0156-9
34. Fortuna, L.; Frasca, M.; Rizzo, A. Chaos preservation through continuous chaotic pulse position modulation. The 2001 IEEE International Symposium on Circuits and Systems, Sydney, NSW, Australia, 6-9 May 2001, pp. 803-806. https://ieeexplore.ieee.org/abstract/document/921454
35. Li, J.; Guo, T.; Leung, H.; Xu, H.; Liu, L.; Wang, B.; Liu Y. Locating Underground Pipe Using Wideband Chaotic Ground Penetrating Radar. *Sensors* **2019**, 19, 2913. https://www.mdpi.com/1424-8220/19/13/2913
36. Moser, M.S. Bathymetric uncertainty model for the L-3 Klein 5410 sidescan sonar. University of New Hampshire, Durham, 2009. https://scholars.unh.edu/thesis/451/